Methodologies for the design of LCC voltage-output resonant converters

M.P. Foster, H.I. Sewell, C.M. Bingham, D.A. Stone and D. Howe

Abstract: The paper presents five structured design methodologies for third-order LCC voltage-output resonant converters. The underlying principle of each technique is based on an adaptation of a FMA equivalent circuit that accommodates the nonlinear behaviour of the converter. In contrast to previously published methods, the proposed methodologies explicitly incorporate the effects of the transformer magnetising inductance. Furthermore, a number of the methodologies allow the resonant-tank components to be specified at the design phase, thereby facilitating the use of standard off-the-shelf components. A procedure for sizing the filter capacitor is derived, and the use of error mapping, to identify parameter boundaries and provide the designer with a qualitative feel for the accuracy of a proposed converter design, is explored.

List of symbols

C_f	filter capacitance (F)
C_p	parallel capacitance (F)
C_s	series capacitance (F)
C_{tot}	total equivalent-circuit capacitance (F)
C_η	equivalent load capacitance (F)
P_f	power factor
$\hat{I}_{in}$	peak input current (A)
I_{out}	output current (A)
k	rectifier coefficient
L_m	transformer magnetising inductance (H)
L_s	series inductance (H)
M_i	resonant circuit to output-current ratio
M_v	voltage-conversion ratio
n	transformer-turns ratio
P_{out}	output power (W)
Q	equivalent-circuit quality factor
Q_{Cf}	charge flowing through C_f (C)
R_L	load resistance (Ω)
R_η	equivalent load resistance (Ω)
V_b	rectifier input voltage (V)
v_{cp}	parallel capacitor voltage (V)
V_{dc}	DC input voltage (V)
V_{out}	output voltage (V)
Z_{tot}	total equivalent-circuit impedance (Ω)
α	percentage-ripple-voltage specification
δ_1	rectifier nonconduction period (s)
δ_2	C_f charging duration (s)
θ_1	rectifier nonconduction angle (°)
ω_0, f_0	resonant frequency (rads^{-1}, Hz)
ω_n, f_n	normalised switching frequency (rads^{-1}, Hz)
ω_s, f_s	switching frequency (rads^{-1}, Hz)

IEE Proceedings online no. 20050357
doi:10.1049/ip-epa:20050357
Paper first received 6th September and in final revised form 6th December 2005

M.P. Foster, C.M. Bingham, D.A. Stone and D. Howe are with the Electrical Machines and Drives Group, Department of Electronic and Electrical Engineering, University of Sheffield, Mappin Street, Sheffield S1 3JD, UK
H.I. Sewell is with Inductelec Ltd., Sheffield, UK
E-mail: m.p.foster@sheffield.ac.uk

1 Introduction

Increasingly, resonant power converters are becoming the preferred technology for a wide variety of industrial, commercial- and consumer-product applications, owing mainly to their high power density. In part, this is facilitated by a reduction in component size, due to the use of high switching frequencies and the reduced heat-sinking requirements, which results from their increased efficiency. Additionally, resonant converters offer the possibility of exploiting transformer parasitics, such as the magnetising inductance, leakage inductance and interwinding capacitance, directly in the resonant tank circuit, thereby reducing the need for discrete components. Indeed, several component manufacturers have recognised the commercial potential of resonant converters, and are producing dedicated resonant-converter-controller integrated circuits.

Although many resonant-converter topologies have been investigated in the literature, it is the LCLC family of converters that has received the most attention. Particular members of the LCLC family offer significantly superior open- and short-circuit behaviour compared with second-order counterparts, with some also exhibiting load-independent operating points [1, 2]. However, in contrast to second-order variants, the analysis and design of these third-order converters is complicated by the requirement to model more than one useful mode of operation.

Although the use of fundamental-mode-approximation (FMA) techniques for the analysis and design of resonant converters [1–3] has been widespread, they suffer from a number of limitations. First, as the switching frequency moves away from the resonant frequency, the tank-current waveform becomes increasingly triangular, thereby invalidating the sinusoidal-waveform assumption which is implicit in the use of FMA. Secondly, the number of circuit states that exist during a single switching cycle can change with the operating condition. The LCC current-output

converter, for example, exhibits significant nonlinear behaviour when heavily loaded [4], leaving the designer with a degree of uncertainty as regards the appropriateness of the chosen equivalent circuit. In an attempt to address such issues, 'modified' FMA equivalent circuits, that more accurately represent the waveshape of a particular variable, have been developed. In [4], for instance, an equivalent-circuit model for the LCC current-output converter operating under heavy- and intermediate-load conditions was developed, by extracting the fundamental component from an equation which described the nonsinusoidal parallel capacitor voltage. Other design/analysis methodologies based on state–space models have also been reported, although they generally require the solution of nonlinear simultaneous equations, which often requires recourse to numerical methods and/or design charts [5, 6].

In this paper, five novel design-synthesis methodologies for LCC voltage-output converters are presented. All the techniques enable the values of the resonant-circuit components to be determined given a specified voltage-conversion factor, and a further specification particular to the chosen methodology. The equivalent circuit is defined entirely in closed form, thereby making the procedures deterministic, and recourse to interpolation or complex numerical solutions is not required. Further, a procedure for sizing the filter capacitor is derived based on the equivalent-circuit model. The paper also introduces the concept of confidence mapping to provide a mechanism for assessing the accuracy of the results generated from a particular design procedure, and give the designer a means of fine tuning a converter's performance. Thus, it has the potential to reduce the design effort significantly, particularly during the initial phases, by identifying the viability of a particular converter design and reducing the number of simulation verification steps which are normally required.

To reduce the complexity of the proposed design methodologies, the following assumptions are made:

(i) All the passive components behave linearly;

(ii) Diodes are ideal one-way switches with an on-state voltage drop;

(iii) MOSFETs are ideal switches with zero on-state resistance;

(iv) All switches commutate instantaneously; and

(v) The converter input voltage is constant.

2 Equivalent-circuit modelling of LCC voltage-output converter

Consider the LCC voltage-output converter shown in Fig. 1 in which the half-bridge MOSFETs T_1 and T_2 are switched in antiphase at a frequency f_s, thereby effectively 'chopping' the DC link voltage V_{dc} to produce a square-wave input voltage V_i to the resonant tank. This excites the resonant tank and causes current i_{in} to flow. The output voltage V_{out} is developed from the portion of i_{in} which flows into the filter capacitor C_f when the rectifier is conducting, during which time the parallel capacitor voltage v_{cp} is clamped to V_{out}. When i_{in} crosses zero, the rectifier turns off and v_{cp} falls (or rises) from V_{out} ($-V_{out}$) with a negative (positive) slope. When $v_{cp} = -V_{out}$, the rectifier commutates and clamps v_{cp} at $-V_{out}$. The rate at which v_{cp} charges/discharges is determined by the values of C_p and R_L.

The behaviour of the LCC converter is similar to that of the classical series-resonant converter [1, 3], with the exception that the rate-of-change of voltage at the input

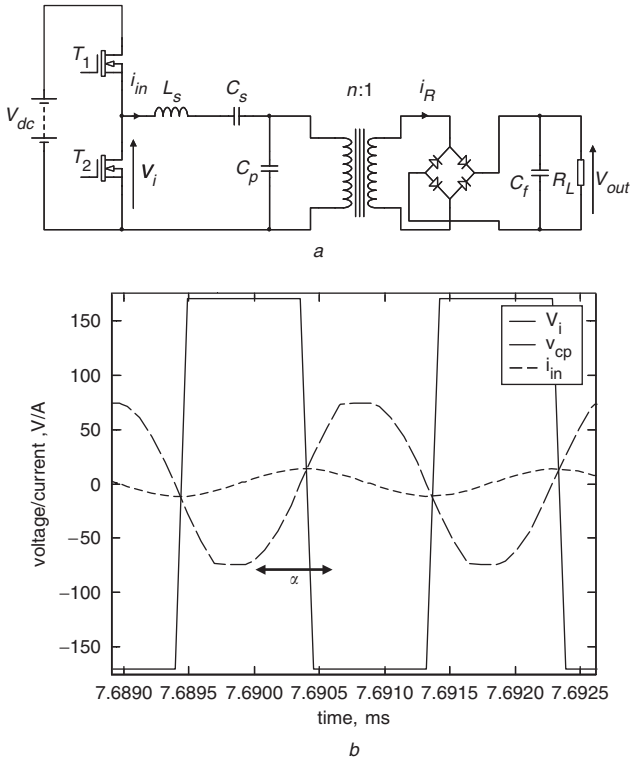

Fig. 1 *LCC voltage-output converter*
a Converter
b Component waveforms

to the bridge rectifier is limited by the presence of C_p. Moreover, it can be shown [6–9] that the interaction between C_p and C_f via the rectifier can produce a voltage gain greater than unity, a feature which is not possible with a classical second-order series converter.

Although the series-resonant converter is readily analysed using FMA by replacing V_{dc} by an equivalent sinusoidal voltage and representing the load and rectifier by an equivalent resistor R_e, in practice this is not appropriate for the LCC voltage-output-converter variant since v_{cp} cannot be assumed to have either a square or sinusoidal waveform, owing to the dv/dt-limiting effect of C_p. Consequently, a describing function is used to model v_{cp} as a complex voltage source, that is ultimately transformed into an 'equivalent' complex impedance. This paper follows the approaches taken in [7, 8], with the exception that equivalent-circuit passive components are derived explicitly and the effect of the rectifier on-state voltage is considered. The proposed analysis begins by assuming that the tank-current waveform is sinusoidal, i.e.

$$i_{in} = \hat{I}_{in} \sin(\omega_s t) \tag{1}$$

where $\hat{I}_{in}$ is the peak value of i_{Ls} and $\omega_s = 2\pi f_s$ is the angular switching frequency. This is justified since the filtering action of the tank circuit removes high-order harmonics, effectively forcing the input current to be a sinusoid.

While the rectifier is conducting, the parallel capacitor voltage is clamped to the output voltage, and is described by

$$v_{cp} = n(V_{out} + kV_d)\text{sgn}(i_{Ls}) \tag{2}$$

where $k = 1$ for a half-bridge rectifier or $k = 2$ for a full-bridge rectifier.

From Fig. 1*b*, the rectifier switches off when the resonant-circuit current, i_{in}, crosses zero, at which time i_{in} starts to charge C_p. The period during which C_p is charging

can be obtained from the solution of

$$v_{cp} = v_{cp\_0} + \frac{1}{C_p}\int_0^{\delta_1} \hat{I}_{in}\sin(\omega_s t)dt \tag{3}$$

where δ_1 defines the end of the diode nonconduction period and $v_{cp\_0}\}$ is the initial voltage on C_p. Solving for v_{cp} for the case when the initial condition is $v_{cp\_0} = -nV_b = -n(V_{out} + kV_d)$ gives

$$v_{cp} = -nV_b + \frac{\hat{I}_{in}}{\omega_s C_p}\{1 - \cos(\omega_s t)\} \tag{4}$$

The charging time (or nonconduction period) can be found by solving (4) for δ_1 to give

$$\delta_1 = \frac{1}{\omega_s}\cos^{-1}\left(1 - \frac{2n\omega_s V_b C_p}{\hat{I}_{in}}\right) = \frac{1}{\omega_s}\theta_1 \tag{5}$$

where $\theta_1 = \cos^{-1}\{1 - (2n\omega_s V_b C_p/\hat{I}_{in})\}$.

The converter's output current I_{out} is obtained by determining the average current flowing through the rectifier during a complete cycle. Defining the angle at which the rectifier starts to conduct as θ_1, the output current is found from

$$\begin{aligned} I_{out} &= \frac{n}{2\pi}\left\{\int_{\theta_1}^{\pi}\hat{I}_{in}\sin(\theta)d\theta + \int_{\theta_1+\pi}^{2\pi} -\hat{I}_{in}\sin(\theta)d\theta\right\} \\ &= \frac{2n}{\pi}(\hat{I}_{in} - V_b\omega_s C_P) \end{aligned} \tag{6}$$

The output voltage is then readily determined from Ohm's law:

$$V_{out} = 2nR_L\left(\frac{\hat{I}_{in} - kn\omega_s C_P V_d}{\pi + 2n^2 R_L\omega_s C_P}\right) \tag{7}$$

To calculate V_{out}, $\hat{I}_{in}$ must be determined from the impedance that the converter presents to the source. To facilitate this, v_{cp} is converted into a complex voltage source using describing-function techniques. Using (2)–(5), v_{cp} is described over a full cycle by

$$v_{cp} = \begin{cases} -nV_b + \dfrac{\hat{I}_{in}}{\omega_s C_p}\{1 - \cos(\theta)\} & 0 \le \theta < \theta_1 \\ nV_b & \theta_1 \le \theta < \pi \\ nV_b - \dfrac{\hat{I}_{in}}{\omega_s C_p}\{1 + \cos(\theta)\} & \theta_1 \le \theta < \theta_1 + \pi \\ -nV_b & \theta_1 + \pi \le \theta < 2\pi \end{cases} \tag{8}$$

The describing function for v_{cp} is obtained by extracting the fundamental from the Fourier series of (8). Substituting for V_b and θ_1 and subsequently dividing by $\hat{I}_{in}$ gives the equivalent impedance Z_e seen by the resonant circuit. Separating the equivalent impedance Z_e into a resistive component R_η and a capacitive component C_η gives

$$\begin{aligned} R_\eta &= \frac{4(2nR_L I_{in} + k\pi V_d)(I_{in} - 2n\omega_s C_p V_d)}{\gamma^2 I_{in}^2} \\ C_\eta &= \pi\gamma C_p I_{in}\Big/\left(\frac{2}{\gamma I_{in}}\sqrt{\{n\pi\omega_s C_p(2nR_L I_{in} + k\pi V_d)(I_{in} - 2n\omega_s C_p k V_d)\}}\right. \\ &\quad \times \{I_{in}(\gamma - 2\pi) + 2n\pi\omega_s C_p k V_d\} \\ &\quad \left. + I_{in}\gamma\left[\pi - \cos^{-1}\left\{\frac{(\gamma - 2\pi)I_{in} + 2n\pi\omega_s C_p k V_d}{\gamma I_{in}}\right\}\right]\right) \end{aligned} \tag{9}$$

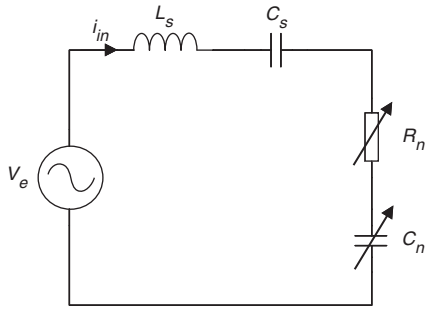

Fig. 2 *Equivalent circuit for LCC voltage-output converter*

where $\gamma = \pi + 2\omega_s C_p n^2 R_L$. Further information regarding the derivation of R_η and C_η is given in [8].

Inserting the series combination of R_η and C_η in place of C_p and its parallel components yields the equivalent series circuit for the converter shown in Fig. 2.

From standard circuit analysis, the total impedance Z_{tot} is given by

$$\begin{aligned} Z_{tot} &= Z_e + j\left(\omega_s L_s - \frac{1}{\omega_s C_s}\right) \\ &= R_\eta + j\left(\omega_s L_s - \frac{C_s + C_\eta}{\omega_s C_s C_\eta}\right) \\ &= R_\eta + j\left(\omega_s L_s - \frac{1}{\omega_s C_{tot}}\right) \end{aligned} \tag{10}$$

Hence, the magnitude of the input current, $\hat{I}_{in}$, is obtained from Ohm's law as

$$\hat{I}_{in} = \frac{V_e}{|Z_{tot}|} \tag{11}$$

The output voltage is obtained by substituting (11) into (7).

For analysis purposes, the calculation of C_η and R_η is reliant on $\hat{I}_{in}$, which is not generally known *a priori*. However, by setting $V_d = 0$ in (5), (9), (10) and (11), an initial estimate for $\hat{I}_{in}$ (denoted with a prime) is obtained iteratively, as follows:

$$\begin{aligned} R'_\eta &= \frac{8n^2 R_L}{\gamma^2} \\ C'_\eta &= \frac{\pi\gamma^2 C_p}{2n\sqrt{(2\pi\omega_s C_p R_L)(\gamma - 2\pi) + \gamma^2\left\{\pi - \cos^{-1}\left(\dfrac{\gamma - 2\pi}{\gamma}\right)\right\}}} \end{aligned} \tag{12}$$

The total impedance seen at the source is therefore estimated to be

$$Z_{tot} = R'_\eta + j\left(\omega_s L_s - \frac{1}{\omega_s C'_{tot}}\right) \tag{13}$$

An initial estimate of the input current immediately follows from (13), i.e.

$$\hat{I}'_{in} = \frac{(2/\pi)V_{dc}}{\sqrt{\left\{R'^2_\eta + \left(\omega_s L_s - \dfrac{1}{\omega_s C'_{tot}}\right)^2\right\}}} \tag{14}$$

Once $\hat{I}'_{in}$ has been determined, an estimate of V_{out} can subsequently be refined using the following

procedure:

(*a*) Substitute $\hat{I}'_{in}$ and V_d into (5), (9), (10) and (11) to obtain a revised value for $\hat{I}_{in}$.

(*b*) Return to step 1 for the next iteration, or after convergence go to step 3.

(*c*) Finally, use the refined value of $\hat{I}_{in}$ to determine V_{out} using (7).

Numerous simulation studies have shown that the foregoing iterative refinement procedure converges rapidly, with very little improvement in the results after the third iteration. A more detailed description of the equivalent-circuit model is given in [9].

3 Design methodologies

This Section describes five novel design methodologies based on the equivalent-circuit model presented. In addition, a procedure for incorporating the magnetising inductance of a transformer within the design of a converter, along with a procedure for filter capacitor sizing, are also discussed.

The first methodology (designated DM1) bases the design on standard AC-circuit parameters (Q and ω_0) and the rectifier nonconduction angle θ_1. The second methodology (DM2) employs the definition of the switch power factor, whilst the remaining methods (DM3–5) allow some resonant-circuit values to be specified during the design process, thereby allowing the designer to use standard 'off-the-shelf' components.

As with most design techniques, a standard set of core-specification parameters is required, summarised in Table 1.

Table 1: Standard specification parameters

Parameter	Description
V_{dc}	DC input voltage (V)
V_{out}	DC output voltage (V)
P_{out}	Output power (W)
V_d	Diode on-state voltage (V)

3.1 Design method 1 (DM1): specified rectifier nonconduction angle θ_1

In this method, all the resonant-circuit components (i.e. L_s, C_s and C_p) of the converter are determined for a specific rectifier nonconduction angle θ_1, a given operating frequency f_s and a combined equivalent resonant frequency f_0. Unlike the previously published techniques presented in [6, 7], the resonant-circuit-capacitor ratio (C_p/C_s) is not required, thereby making the interpretation of the design more tangible. However, before presenting the design algorithm in detail, it is instructive to consider how the behaviour of the converter is influenced by these parameters.

Analysis: In a similar manner to the normalising procedure described in [3], the parameters Q, ω_0 and ω_n can be used to derive an expression for the voltage-conversion ratio $M_v = V_o/V_{dc}$, where

$$Q = \frac{1}{\omega_0 C_{tot} R_\eta} = \frac{\omega_0 L_s}{R_\eta}, \quad \omega_0 = \frac{1}{\sqrt{(L_s C_{tot})}}, \quad \omega_n = \frac{\omega_s}{\omega_0} \tag{15}$$

Specifically, from [3], M_v is obtained by combining (14) and (7)—neglecting V_d, substituting into (15) and rearranging using (12), to give:

$$M_v = \frac{V_{out}}{V_{dc}} = \frac{1}{n\{1+\cos(\theta_1)\}} \frac{1}{\sqrt{\left\{1+Q^2\left(\omega_n - \frac{1}{\omega_n}\right)\right\}^2}} \tag{16}$$

By inspection, it can be seen that (16) has a similar form to the standard series-resonant-converter FMA model [1, 3], with the exception that the gain is modified by the term $1/[n\{1+\cos(\theta_1)\}]$, which, importantly, shows the potential for having a voltage gain greater than unity, as will be evident from Fig. 3. Moreover, from Fig. 3, it can be seen that the voltage gain increases with the rectifier nonconduction angle. This is expected since, when the rectifier is not conducting, C_p is being charged and can therefore support a greater voltage if charged for longer. Furthermore, Fig. 3 shows that, while the magnitude of the voltage gain at resonance is unaffected by the Q-factor, the bandwidth, and hence the rate at which the voltage gain changes with frequency, is significantly affected. This imposes restrictions on the maximum value of Q that can be employed in terms of the converter controllability and sensitivity to component tolerances.

Although Fig. 3 provides useful information regarding the voltage transfer and control characteristics of an LCC converter, the designer is invariably also required to optimise converter efficiency. However, rather than entering into a detailed discussion about the resonant tank, transformer and rectifier efficiencies (details of which can be found elsewhere [1]), the ratio of the resonant-circuit current to the output current M_i will be used as a metric for design. Setting $V_d = 0$ in (7), and substituting $V_{out} = I_{out}R_L$, using RMS quantities and rearranging, gives

$$M_i = \frac{\hat{I}_{in\_rms}}{I_{out}} = \frac{\pi}{\sqrt{2n\{1+\cos(\theta_1)\}}} \tag{17}$$

Again, by ignoring the transformer turns ratio, it can be seen that M_i is dependent only on θ_1. From Fig. 4, it can clearly be seen that the resonant-circuit current increases significantly for $\theta_1 > 90°$. Further, from Fig. 3, it can be seen that, to achieve a voltage gain greater than unity at resonance, $\theta_1 > 90°$.

To summarise, Q should be chosen to reduce problems associated with component-tolerance sensitivity and controllability issues, and θ_1 should be chosen to reduce the circulating current in the tank circuit, thereby reducing conduction losses in the switches and inductor, and to minimise voltage/current stresses on individual components. Consequently, for a step-down converter, $\theta_1 < 90°$, whilst for step-up operation, the designer must trade off the effects of an increase in transformer turns ratio with circulating-current levels. A suitable value for θ_1, having been chosen, together with nominal values for ω_s and ω_0, specific component values can be determined.

Design procedure: The load resistance is calculated from

$$R_L = \frac{V_{out}}{I_{out}} \tag{18}$$

where $I_{out} = P_{out}/V_{out}$. A value for C_p is then obtained by solving (6) for $\hat{I}_{in}$, and substituting into (5). After rearrangement, this gives

$$C_p = \frac{\pi I_{out}}{2n\omega_s V_b} \frac{1-\cos(\theta_1)}{2n-1+\cos(\theta_1)} \tag{19}$$

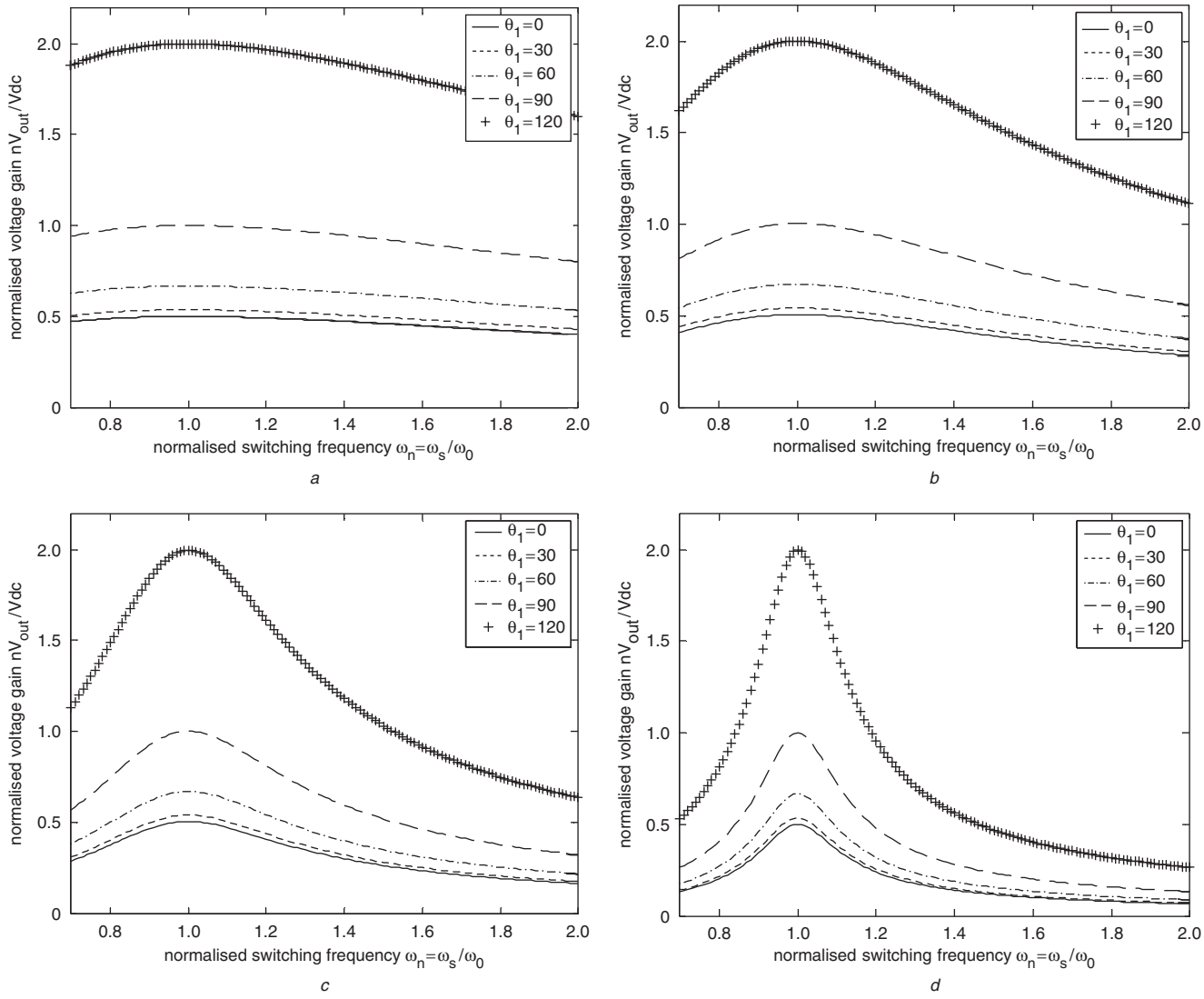

Fig. 3 *Converter-voltage transfer ratio for varying Q-factors*
a $Q = 0.5$
b $Q = 1$
c $Q = 2$
d $Q = 5$

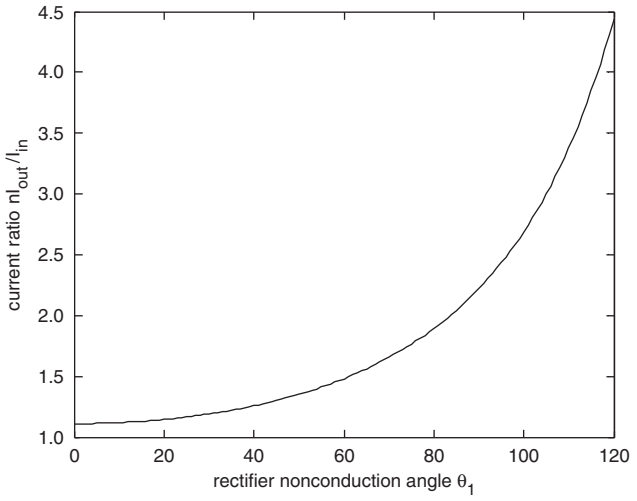

Fig. 4 *Resonant-circuit current-to-output current ratio*

Since the equivalent-circuit components R_η and C_η are defined entirely in terms of the design parameters f_s, R_L and C_p, they can immediately be found from (9).

Subsequently, L_s and C_s are determined from the required impedance of the equivalent resonant circuit which is necessary to achieve a specific input current, where

$$\hat{I}_{in} = \frac{\pi I_{out}}{n\{1 + \cos(\theta_1)\}} \tag{20}$$

The total circuit capacitance, C_{tot}, is obtained by rearranging (14) and substituting into (15) to give

$$C_{tot} = \frac{\omega_n^2 - 1}{\omega_s \sqrt{\left\{ \frac{4}{\pi^2} \left(\frac{V_{dc}}{\hat{I}_{in}} \right)^2 - R_\eta^2 \right\}}} \tag{21}$$

Since C_η is obtained from (9), C_s can be determined from

$$C_s = \frac{C_\eta C_{tot}}{C_\eta - C_{tot}} \tag{22}$$

Finally, the series inductance is found from the definition of the converter resonant frequency (15), namely

$$L_s = \frac{1}{\omega_0^2 C_{tot}} \tag{23}$$

3.2 Design method 2 (DM2): specified switch power factor

In this approach, the resonant-circuit component values are calculated to achieve a specified switch power factor at the specified switching frequency, given a maximum voltage stress on C_s.

An initial estimate for the peak resonant current $\hat{I}'_{in}$ is obtained from the output power, the power factor $P_f = \cos\phi$ and the RMS value of the input voltage is $(\sqrt{2}/\pi)/V_{dc}$, as follows:

$$\hat{I}'_{in} = \frac{\pi P_{out}}{V_{dc} P_f} \tag{24}$$

The power loss P_{loss} in the circuit is then estimated from

$$P_{loss} = 2V_d I_{out} + \frac{\hat{I}'^2_{in} R_s}{2} \tag{25}$$

where R_s is an 'optional' series resistance. The total input power is then obtained from

$$P_{in} = P_{out} + P_{loss} \tag{26}$$

By replacing P_{out} with P_{in} in (24), a revised value for $\hat{I}_{in}$ is obtained as

$$\hat{I}_{in} = \frac{\pi P_{in}}{V_{dc} P_f} \tag{27}$$

The improved estimate of $\hat{I}_{in}$ is then substituted into (25), and the refinement process is repeated. Again, it has been shown that a maximum of three iterations is usually sufficient to obtain results which are accurate to three significant figures.

R_η and C_η are found from (9), and C_p is obtained by rearranging (6):

$$C_p = \frac{\hat{I}_{in}}{\omega_s V_b} - \frac{\pi I_{out}}{2n\omega_s V_b} \tag{28}$$

C_s is obtained by specifying the maximum allowable voltage stress $\hat{V}_{cs}$ and the peak tank current:

$$C_s = \frac{\hat{I}_{in}}{\omega_s \hat{V}_{Cs}} \tag{29}$$

giving the total equivalent-circuit capacitance:

$$C_{tot} = \frac{C_s C_\eta}{C_s + C_\eta} \tag{30}$$

L_s is then found from (23).

3.3 Design method 3 (DM3): specified C_p

The remaining design methodologies are particularly useful if the designer is constrained in the choice of component values. In this particular case, L_s and C_s are calculated when the value of C_p is fixed. The method is based on DM1 in which the peak input current was used to determine L_s and C_s.

Initially, R_L is calculated from (18) and the peak input current $\hat{I}_{in}$ is found by rearranging (6) and inserting values for the switching frequency and C_p:

$$\hat{I}_{in} = \frac{\pi I_{out} + 2nV_b\omega_s C_p}{2n} \tag{31}$$

Values of L_s and C_s are then determined from (21)–(23).

3.4 Design method 4 (DM4): specified L_s

To begin with, a value of C_p is selected based on either DM1 or DM2; C_s is then readily determined from L_s, ω_s and ω_0:

Method 1: Specified diode non-conduction angle

Using θ_1, C_p is obtained directly from (19).

Method 2: Specified switch power factor

The peak input current is found by solving (25)–(27) iteratively. Once $\hat{I}_{in}$ has converged, C_p is calculated using (31).

C_p having been determined the total circuit capacitance is given by:

$$C_{tot} = \frac{1}{\omega_0^2 L_s} \tag{32}$$

from which C_s is found by substituting (9) into (22).

3.5 Design method 5 (DM5): specified C_s and C_p

In this method, a value of L_s is sought from the specification of C_p, C_s, ω_s and ω_0 by employing (25)–(27) to determine the input current in an iterative manner. Subsequently, (9) is used to calculate the equivalent components R_η and C_η. The total circuit capacitance is then deduced from (30) and, finally, the required value of L_s is determined from (32).

Although a designer may elect to use any of the foregoing design methodologies to determine the tank components for a specific resonant converter, certain methodologies lend themselves to particular applications. Specifically, methodology DM1 is appropriate when attempting to minimise the EMI generated by a converter, since the rectifier nonconduction angle θ_1 determines the noise level which is generated by the rectifier. For small values of θ_1, the waveform of v_{Cp} resembles a square wave, and therefore has a large harmonic content. However, for large values of θ_1, v_{Cp} tends to a sinusoid with a much lower harmonic content. Thus, a designer can vary θ_1 so as to minimise EMI. Methodology DM2 is more appropriate when efficiency is a key consideration, since the procedure explicitly accounts for the power losses associated with the rectifier diodes, the MOSFET on-state resistance and other parasitic resistances which are present in the tank circuit at the design stage. This methodology also allows the maximum voltage across C_s to be specified during the design process. Design methodologies DM3–DM5 would be employed when a designer is required to use 'off-the-shelf' circuit components.

3.6 Inclusion of transformer parasitics

Although an LCC converter can be designed to provide a voltage-boost capability, the requirement for a significant step-up voltage conversion will often require the incorporation of a transformer and, from a commercial perspective, the use of an isolation transformer is often required for reasons of safety. The effects of transformer magnetising inductance L_m can be included in a design by modifying tank-circuit-current calculation. This is accomplished by:

(i) Initially, neglect L_m and calculate an initial value, $\hat{I}_{in\_initial}$, of $\hat{I}_{in}$ from (20), (24) or (31), depending on the design methodology.

(ii) Using $\hat{I}_{in}$, determine values for the equivalent components R_η and C_η using (9).

(iii) Calculate the fundamental component of v_{cp}, from $v_{cp\_1} = \hat{I}_{in}\left(R_\eta + \frac{1}{sC_\eta}\right)$, where $s \rightarrow j\omega_s$.

(iv) Determine the current drawn by L_m, from $I_{Lm} = \frac{v_{cp\_1}}{j\omega_s L_M}$.

(v) Calculate a revised value $\hat{I}_{in\_new}$ for the input current, from $\hat{I}_{in\_new} = \hat{I}_{in\_initial} + \hat{I}_{Lm}$.

(vi) Determine the resonant-circuit components, as before, using $\hat{I}_{in\_new}$.

3.7 Filter-capacitor sizing

In general, the value of C_f is chosen to satisfy the output-voltage-ripple specification, such that the ripple does not exceed α%. A suitable value for C_f is calculated by considering the charge which flows into C_f and the corresponding voltage rise over a specific time interval. From the example waveforms shown in Fig. 5, it can be seen that, during the rectifier conduction period, the current which flows into C_f is the difference between the rectifier input and output currents.

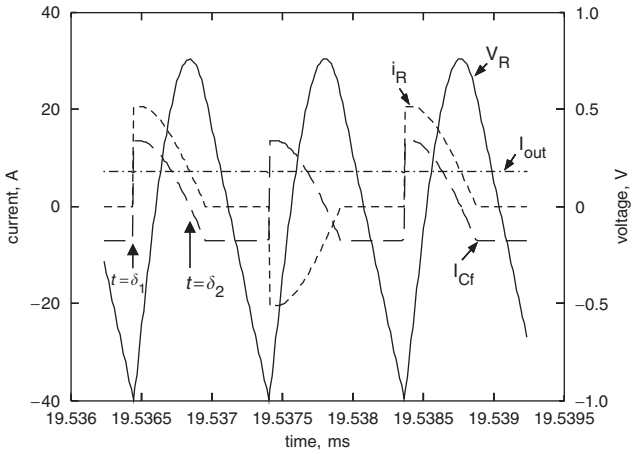

Fig. 5 *Voltage and current waveforms for filter capacitor*

Considering the period during which current is replenishing the charge on C_f, then

$$Q_{Cf} = \int_{\delta_1}^{\delta_2} i_{Cf}\,dt = \int_{\delta_1}^{\delta_2} \{n\hat{I}_{in}\sin(\omega_s t) - I_{out}\}dt \qquad (33)$$

where δ_2 is the time at which i_{Cf} becomes zero. δ_2 is found from the solution of:

$$i_{Cf} = n\hat{I}_{in}\sin(\omega_s t) - I_{out} = 0$$

Therefore

$$\delta_2 = \frac{1}{\omega_s}\left\{\pi - \sin^{-1}\left(\frac{I_{out}}{n\hat{I}_{in}}\right)\right\} \qquad (34)$$

During this period V_{out} increases by an amount v_{rip}, which provides a further expression for the charge flowing into C_f:

$$Q_{Cf} = C_f v_{rip} = C_f \alpha V_{out} \qquad (35)$$

The minimum value of C_f which is required to limit v_{rip} to a specified level α is found by equating (33) and (35), and rearranging to give

$$C_f > \frac{n\hat{I}_{in}}{\alpha V_{out}\omega_s}\{\cos(\omega_s\delta_1) - \cos(\omega_s\delta_2)\} - \frac{1}{\alpha R_L}(\delta_2 - \delta_1) \qquad (36)$$

If $V_{out} \gg V_d$, (36) reduces to

$$C_f > \frac{1}{2\alpha R_L\omega_s}\left[\sqrt{(\gamma^2-4)} - \gamma + 2\left\{\cos^{-1}\left(\frac{\gamma - 4R_L\omega_s C_P}{\gamma}\right) + \sin^{-1}\left(\frac{2}{\gamma}\right)\right\}\right] \qquad (37)$$

3.8 Experimental verification

To demonstrate the validity of the proposed design methodologies, a 25 V-input, 35 V-output, 22 W experimental converter was designed to meet the specification outlined in Table 2 using DM4. The component values for the remaining resonant-circuit components were determined, using DM4, as $C_p = 89$ nF, $C_s = 224$ nF while the value for C_p was realised by paralleling four 22 nF capacitors to give 87 nF measured and the value for C_s created from a 220 nF capacitor was connected in parallel with two 2.2 nF capacitors giving 224 nF measured.

Table 2: Prototype converter parameters

Parameter	V_{dc} (V)	V_{out} (V)	P_{out} (W)	L_s (μH)	f_s (kHz)	f_{0s} (kHz)	Q	θ_1 (deg)	n
Value	25	35	22	18.4	150	136	5.5	120	1

Operating as specified (i.e. with $f_s = 150$ kHz), the converter had an output voltage of 33.6 V which was within 5% of the specification. Figure 6 shows the time-domain waveforms of the input voltage to the tank (V_i) and the parallel capacitor voltage (v_{Cp}). Inspection of Fig. 6 shows the diode nonconduction period θ_1 to be $\sim 123^\circ$, which is close to the desired 120°.

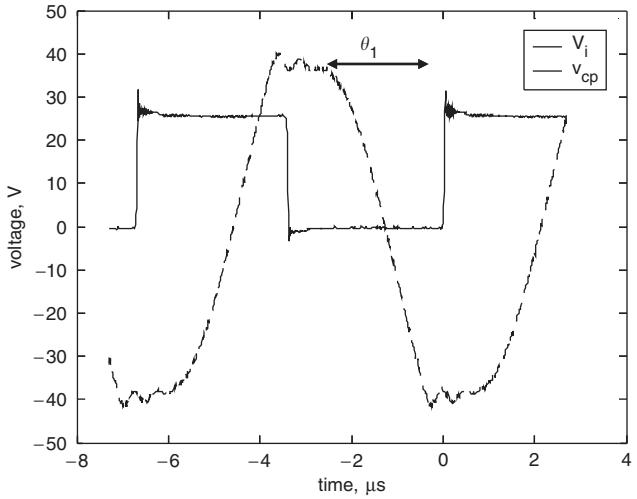

Fig. 6 *Voltage waveforms for prototype 22 W LCC voltage-output converter*

4 Accuracy bounds

Classically, all FMA-based design methodologies assume that voltage and current waveforms can readily be approximated to sinusoids or square waves to simplify circuit analysis. For the analysis described in this paper, the resonant circuit is assumed to respond only to the fundamental component of the input-voltage waveform (because of the filtering attributes of the tank) and a sinusoidal current is therefore assumed to flow in the resonant circuit. However, for switching frequencies much higher than the resonant frequency (and for particular load ranges), the tank current becomes distorted, tending to a triangular waveshape, and thereby contravenes the FMA sinusoidal assumption. Consequently, there exists only a subset of converter parameters, obtained from FMA results, that provide realisable converters having the expected performance characteristics (see the account given [1], for instance).

Table 3: Confidence-map-parameter ranges

Parameter	V_{dc} (V)	Q_s	C_p/C_s	Z_0	f_{0s} (kHz)	f_s	V_d (V)
Value	1–100	1–10	0.01–100	0.01–100	100	(1–2) × f_r	0.45

Here then, a comprehensive investigation is presented to determine parameters that affect prediction performance significantly, by comparing results from over 250 000 simulation studies, obtained from an accurate nonlinear state-variable model of the converter [10], with those from the equivalent-circuit model presented in Section 2, over a bounded range of typical parameter values—specifically, V_{dc}, Z_0, the Q-factor, the ratio C_p/C_s and ω_0. The ranges are summarised in Table 3. From the comparison of results, errors maps are generated to provide an indication of the expected accuracy of a specific converter design. Justification for using the nonlinear-state-variable model as a benchmark metric is that no restrictions regarding the circuit-voltage/current waveshapes or the interaction between the output filter, rectifier and tank, are present, and it is therefore not constrained by underlying assumptions of FMA.

By appropriate manipulation of the resulting data, so-called '2-D confidence maps' that show the impact of each design parameter on the 'confidence' of a particular converter design giving the expected performance, are generated. Since the parameters are applied to the equivalent-circuit model presented in Section 2, the resulting confidence maps can be employed generically. In this case, the data are presented in a manner that can be applied iteratively in conjunction with design procedure DM1; see Figs. 7–9. Although it is recognised that this type of statistical analysis only indicates relative trends, the body of evidence suggests that clearly defined regions of parameter ranges exist where the designer can have a high 'confidence' in realising expected performance from a particular design procedure. For use with DM1, in this example, the diode voltage drop is assumed constant, (0.45 V) in each case. Note that the normalised parameters that have been selected in this case are among many that could have been chosen, including those relating to the ratios C_p/C_s and R_L/Z_o, among others.

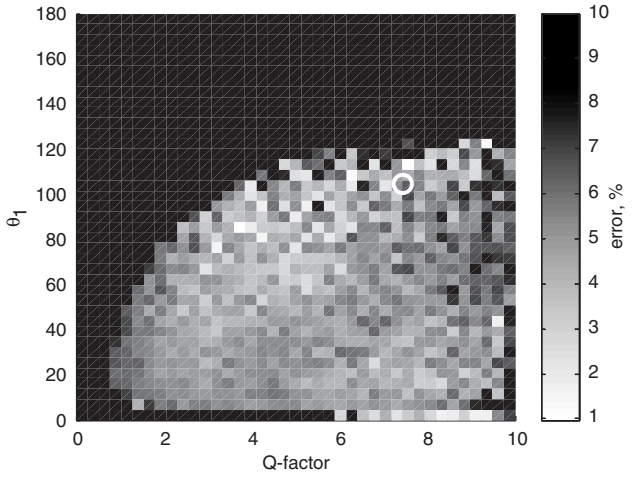

Fig. 7 *Output voltage prediction error as a function of θ_1 and Q-factor*

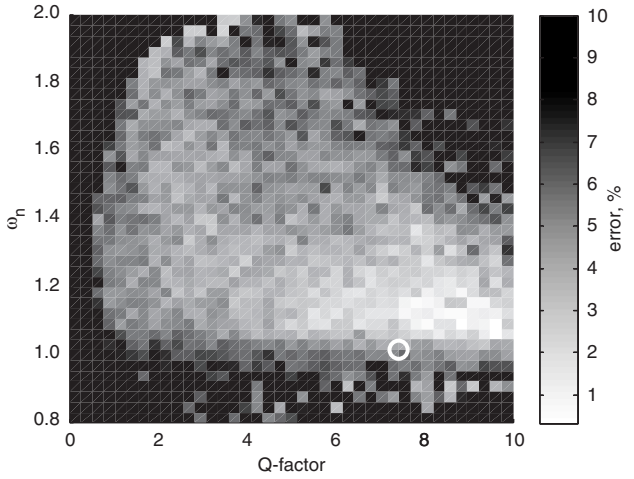

Fig. 8 *Output voltage prediction error as a function of ω_n and Q-factor*

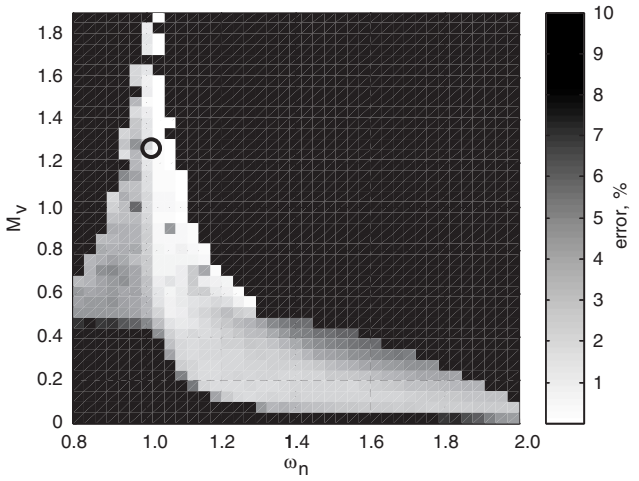

Fig. 9 *Output voltage prediction error as a function of M_v and ω_n*

The procedure for generating the confidence maps is summarised below:

(i) Since, $Q_s = \{(\pi^2/8R_L)\sqrt{(L_s/C_s)}\} = Z_0/R_L$, R_L is calculated.

(ii) Since $\omega_{os} = 1/\sqrt{(L_s/C_s)}$, C_s is calculated from, $C_s = 1/\omega_{0s}Z_0$.

(iii) Using $A = C_p/C_s$, C_p is calculated from $C_p = AC_s$.

(iv) Finally, L_s is determined from $L_s = Z_0^2 C_s$.

The output-filter capacitor for each converter design is selected to limit the ripple on the output voltage to 1%. Finally, the nonlinear-converter model is simulated in the time domain for $10 \times C_f R_L$ seconds to allow sufficient time to achieve steady-state operation.

The variable space on a confidence map is divided into a grid with each 'pixel' representing the level of prediction error (from 0 to 10%), the pixel value being determined by the average 'error' within each element of the grid. The prediction error is calculated from

$$V_{error} = \left| \frac{V_{out} - V_{out\_SS}}{V_{out\_SS}} \right| \times 100\% \quad (38)$$

where V_{out} and V_{out_ss} are the output voltages obtained from the equivalent-circuit model and the state-variable model, respectively.

Figure 7 shows the percentage error between the reference state-variable model and the equivalent-circuit model as a function of the rectifier nonconduction angle θ_1 and the equivalent circuit Q-factor. It can be seen that there exists a definite area, denoted by the dark regions, in which the equivalent-circuit-model predictions become inaccurate. With reference to Fig. 7, to ensure that accurate design predictions can be made using the FMA-based design methodologies, values of $Q>4$ and $\theta_1<120^\circ$ should be chosen. However, limiting the rectifier nonconduction angle $\theta_1<120^\circ$ also restricts the maximum voltage gain of the converter to be less than 2 (see Fig. 3).

Figure 8 shows the prediction error as a function of the ratio of the switching frequency and the 'real' resonant frequency, denoted by ω_n, and the equivalent circuit Q-factor. To have high confidence in realising a converter with the required attributes, it is evident that it should be designed to exhibit a relatively high Q-factor and, correspondingly, should be switched close to the resonant frequency. This conforms to intuitive expectations, since high Q-factor tank circuits provide low-distortion sinusoidal tank currents near resonance. However, as discussed previously, the designer must trade the effects of employing a high Q-factor against the effects on controllability and component sensitivity. Figure 9 shows the design confidence as a function of the voltage-conversion ratio M_v and the Q-factor, and reinforces these findings, since, for instance, confidence is highest for converter designs having $M_v>1$ and $1<\omega_n<1.1$, with the performance of most being within 1% of that predicted from state-variable simulations, as a consequence of the improved filtering of the excitation-voltage harmonics. Moreover, for converter designs requiring $0.5<M_v<1$, the results suggest that ω_n should be <1.3, and, for gains less that 0.5, higher values of ω_n should be chosen to ensure reasonable confidence in realising the expected converter performance.

Although only a small sample of the possible error/confidence mappings have been presented (other key variants include confidence maps as functions of M_v against θ_1 and θ_1 against ω_n), it is apparent that they enable parameter boundaries to be viewed readily, thereby restricting the design space. Moreover, although confidence maps require significant computational effort to generate, ultimately, they are generic, and can be used as an integral part of an interactive design tool. In practice, this is achieved by simultaneously placing a marker on each map at intercepts which correspond to the converter design parameters. The underlying value on the confidence maps then indicates the prediction accuracy. A designer would then interactively modify the converter design parameters so as to achieve a design that satisfied the specification to the required degree of confidence. By way of example, a converter design whose parameters are $L_s=47\,\mu H$, $C_s=22\,nF$, $C_p=33\,nF$, $f_s=190\,kHz$, $V_{dc}=48\,V$, $R_L=70\,\Omega$ and $V_d=0.45\,V$ is superimposed on the confidence maps in Figs. 7–9, from which it can be inferred that this particular design would have an estimated prediction error of approximately 5%. This figure is consistent with the predicted output voltage from the equivalent-circuit and state-variable models, being $V_{out}=63.3\,V$ and $V_{out\_ss}=65.9\,V$, respectively, which correspond to an error of 4%.

5 Conclusions

The paper has presented new approaches for designing LCC voltage-output resonant converters. Specifically, five methodologies for determining the values of the resonant-circuit components, employing various key performance and circuit parameters, including the diode nonconduction angle and the switch power factor, have been investigated. Practical results from a prototype converter have demonstrated the accuracy of the proposed design methodologies. In addition, techniques to account for the effect of the transformer magnetising inductance on the circuit design, and for sizing the filter capacitor, based on an equivalent-circuit model, have been proposed.

The paper has also applied the concept of error mapping. By simulating over 250 000 LCC converter designs over a constrained parameter space, maps of prediction accuracy against design variables have been presented, and their use as an integral part of an interactive design tool has been discussed. Note that, although only a limited number of confidence maps have been included, as a demonstration of principle, ultimately, their generation and use is generic to a wider parameter space, and they can be derived for all other resonant converter variants.

6 References

1 Kazimierczuk, M.K., and Czarkowski, D.: 'Resonant power converters' (John Wiley and Sons, 1995)
2 Steigerwald, R.L.: 'A comparison of half-bridge resonant converter topologies', *IEEE Trans. Power Electron.*, 1988, **3**, (2), pp. 174–182
3 Kazimierczuk, M.K., Thirunarayan, N., and Wang, S.: 'Analysis of series-parallel resonant converter', *IEEE Trans. Aerosp. Electron. Syst.*, 1993, **29**, (1), pp. 88–99
4 Forsyth, A.J., Ward, G.A., and Mollov, S.V.: 'Extended fundamental frequency analysis of the LCC resonant converter', *IEEE Trans. Power Electron.*, 2003, **18**, (6), pp. 1286–1292
5 Batarseh, I.: 'State-plane approach for the analysis of half-bridge parallel resonant converters', *IEE Proc.—Circuits, Devices Systems*, 1995, **142**, (3), pp. 200–204
6 Bhat, A.K.S.: 'Analysis and design of a series-parallel resonant converter with capacitive output filter', *IEEE Trans. Ind. Appl.*, 1991, **27**, (3), pp. 523–530
7 Forsyth, A.J., and Mollov, S.V.: 'Simple equivalent circuit for the series-loaded resonant converter with voltage boosting capacitor', *IEE Proc.—Electr. Power Appl.*, 1998, **145**, (4), pp. 301–306
8 Hayes, J.G., and Egan, M.G.: 'Rectifier-compensated fundamental mode approximation analysis of the series-parallel LCLC family of resonant converters with capacitive output filter and voltage-source load'. Record 30th IEEE Power Electronics Specialist Conf., 1999, Vol. 2, pp. 1030–1036
9 Sewell, H.I., Foster, M.P., Bingham, C.M., Stone, D.A., Hente, D., and Howe, D.: 'Analysis of voltage output LCC resonant converters, including boost mode operation', *IEE Proc.—Electr. Power Appl.*, 2003, **150**, (6), pp. 673–679
10 Foster, M.P., Sewell, H.I., Bingham, C.M., and Stone, D.A.: 'State-variable modelling of LCC voltage output resonant converters', *Electron. Lett.*, 2001, **37**, (17), pp. 1065–1066